Structural Anomaly Detection Using Fiber Optic Sensors and Inverse Finite Element Method

Cuong C. Quach[*] and Sixto L. Vazquez[†], Alex Tessler[‡], Jason P. Moore[§], Eric G. Cooper[**]
NASA Langley Research Center, Hampton, VA, 23681, USA

and

Jan L. Spangler[††]
Lockheed Martin Aeronautics Company, Hampton, Virginia 23681, USA

NASA Langley Research Center is investigating a variety of techniques for mitigating aircraft accidents due to structural component failure. One technique under consideration combines distributed fiber optic strain sensing with an inverse finite element method for detecting and characterizing structural anomalies – anomalies that may provide early indication of airframe structure degradation. The technique identifies structural anomalies that result in observable changes in localized strain but do not impact the overall surface shape. Surface shape information is provided by an Inverse Finite Element Method that computes full-field displacements and internal loads using strain data from in-situ fiber-optic sensors. This paper describes a prototype of such a system and reports results from a series of laboratory tests conducted on a test coupon subjected to increasing levels of damage.

I. Introduction

NASA Langley Research Center (LaRC) has developed technology based upon principles of Optical Frequency-Domain Reflectometry (OFDR) for the provision of large-scale, densely-distributed strain sensors using Fiber Optic Bragg Grating technology (FOBG). This fiber-optic strain sensing (FOSS) technology offers numerous benefits, including low-weight and immunity to electromagnetic interference and moisture. Moreover, the OFDR technique employed enables thousands of FOBG strain sensors, of nominally equivalent wavelength, to be embedded in a single optical fiber. The theory and development of the FOSS technology is described in [1], and the algorithms and methods for deriving strain from an OFDR measurement system are described in [2]. The FOSS technology has been used for in-situ strain sensing during tests conducted on an advanced composite transport wing box [3] and for crack monitoring during a series of lap splice fatigue cycle tests [4].

FOSS provides the strain sensing for a new aerospace vehicle structural health monitoring concept that incorporates anomaly detection using strain measurements and structural deformation characterization using an Inverse Finite Element (iFEM) tool. In this concept, structural anomaly may be detected and located directly from strain data while full-field displacement and internal loads are computed by the iFEM tool.

---

[*] Computer Engineer, Safety Critical Avionics Systems Branch, NASA/Langley Research Center, 1 S Wright St. Hampton, VA 23681.
[†] Electrical Engineer, Safety Critical Avionics Systems Branch, NASA/Langley Research Center, 1 S Wright St. Hampton, VA 23681.
[‡] Mechanical Engineer, Computational Structures and Materials Branch, NASA/Langley Research Center, 1A East Reid St. Hampton, VA 23681.
[§] Electrical Engineer, Safety Critical Avionics Systems Branch, NASA/Langley Research Center, 1 S Wright St. Hampton, VA 23681.
[**] Computer Engineer, Safety Critical Avionics Systems Branch, NASA/Langley Research Center, 1 S Wright St. Hampton, VA 23681.
[††] Computer Scientist, Lockheed Martin Aeronautics Company, Hampton, VA 23681.

This paper presents a brief description of combined FOSS / iFEM as a structural anomaly detection system and reports results from a series of experiments designed to show the feasibility of the combined system to detect anomalies. The report concludes with a discussion of issues and possible areas for further research.

II. FOSS/iFEM system

A prototype FOSS system has been augmented with the iFEM analysis to produce a new technology base for in-situ structural anomaly detection. This section briefly describes the LaRC FOSS system and the iFEM analysis technique. Theoretical basis and specifics about the iFEM technique are found in [5,6].

The FOSS system consists of sensing fibers, an optical network, electro-optic hardware, and data demodulation software as diagrammed in Fig. 1. The sensing fibers are bonded to the surface of, or embedded in, a load-carrying structural member (host structure) and are connected to a wavelength-sweeping laser through the optical network. During an interrogation cycle, the source laser is swept through a preset range of wavelengths and the reflections from the FOBGs are converted to electrical signals by photo-detectors. The converted signals are sampled and transferred to the demodulation software for strain derivation at each FOBG location, as described in detail in [2] and [7].

The iFEM technique reconstructs the full field (every point in the structure) structural displacements based on surface strain measurements which are provided by the FOSS instrumentation. The problem space (structure) is represented using a finite element model whose elements are assigned the measured strains. The displacements are found by solving an inverse problem constructed using variational principle. The iFEM technique is suitable for real-time application and is applicable to thin and moderately thick beams, plates, shells, and built-up structures. The mathematical foundation for the iFEM is described in [5, 6, 8]. Experimental results that show the capability of the iFEM to reconstruct a beam shape using the FOSS is described in [7].

Figure 1. FOSS system diagram.

Figure 2. Test article mounted on optical table.

III. Test Article and Test Aparatus

To asses the feasibility of using the combined FOSS / iFEM system for structural anomaly detection, an experiment was conducted on a simple aluminum bar subjected to increasing levels of damage. The aluminum bar measures 1219.2 mm X 63.5 mm X 6.35 mm as pictured in Fig. 2, with detailed dimensions diagrammed in Fig. 3.
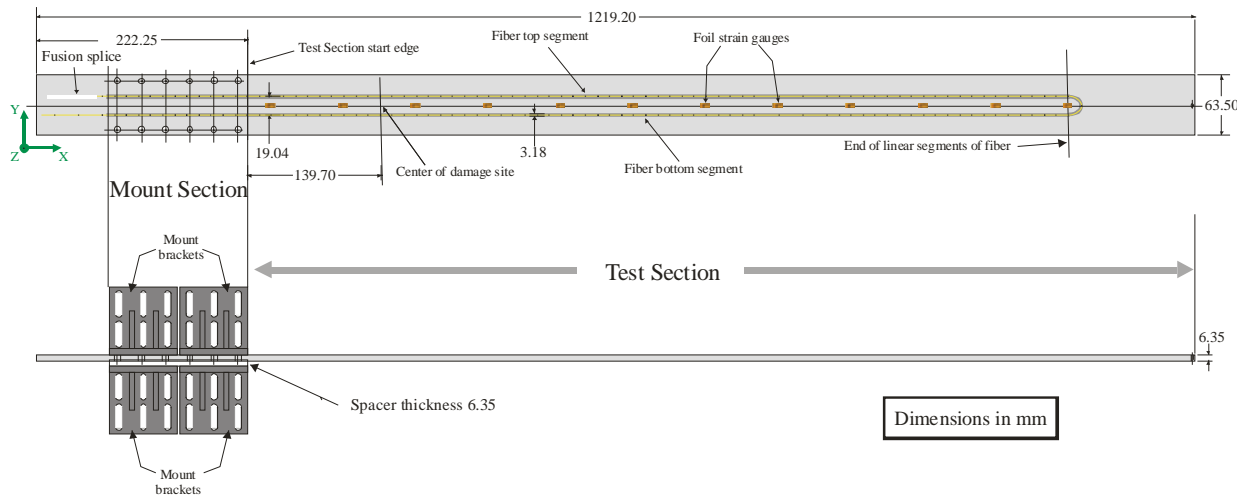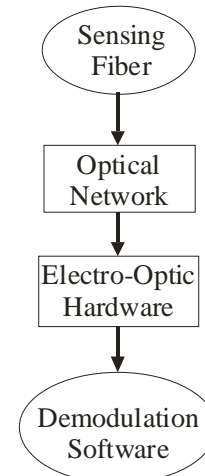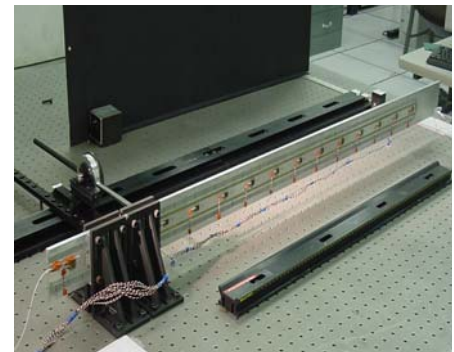

Figure 3. ITA design and sensor layout

American Institute of Aeronautics and Astronautics

A FOSS sensing fiber was bonded to one side of the bar, as diagrammed in Fig. 3, affixed along the length of the bar and looped back to provide two linear sections for measuring strain along the bar's length. The bar was also instrumented with 12 foil-type strain sensors that were distributed along the bar's centerline. There were 134 strain-sensing gratings in the test section, each grating approximately 4 mm long and distributed 12.7 mm apart on center.

The bar was oriented so that the surface with the bonded sensors was orthogonal to gravity. Loading was applied in the ±Z direction using a wire connected to a through hole at the bar tip and connected to a pulley mechanism as shown in the diagram in Fig. 4 and pictured in Fig. 5. During testing, a load was applied to only one side at a time. A load in the +Z direction causes the sensors to read compression and accordingly a load in the -Z causes the sensor to read tension.

Physical displacements were measured using a 5-inch travel linear gauge mounted horizontally so that its probe contacted the instrumented test article (ITA) on the non-instrumented surface as indicated in Fig. 4 and pictured in Fig. 6. Since the probe required contact with the test article, the displacement measurements taken by the probe were corrected to negate the displacement induced by the probe force.
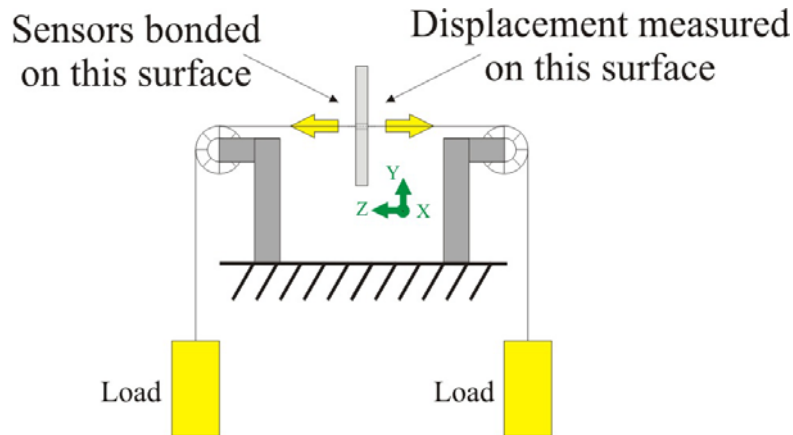

Figure 4. Diagram of loading mechanism.

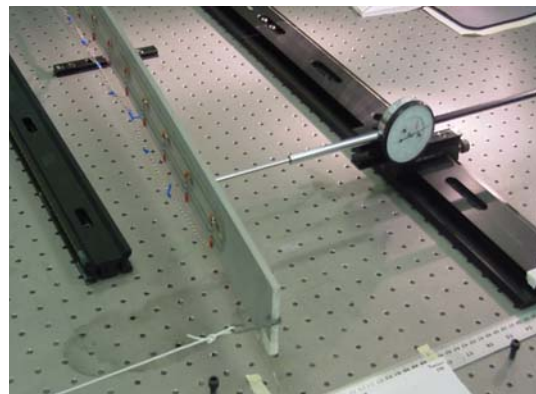
Figure 5. Bar with 1062 gram compression load.

Figure 6. Setup for measuring displacement.

American Institute of Aeronautics and Astronautics

IV. Test Cases

Test cases consisted of subjecting the ITA to nine load cases under five levels of damage. The damage states were (a) no damage, (b) 3.175mm hole, (c) 6.350mm hole, (d) 9.525mm hole, and (e) 12.700mm hole. The damage site (hole), which was drilled, was located approximately 139 mm from the clamped edge and at the center line of the bar (Fig. 7). This distance was chosen to minimize non-ideal cantilever boundary condition effects. The load cases consisted of a zero load, and four compressive / tensile loads as shown in table 1, which organizes the test cases by damage state and load condition. For example, "S-1-C20" refers to
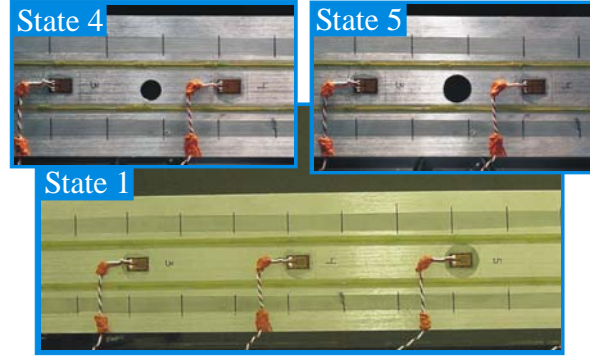
Figure 7. Picture of ITA in 3 of the tested states.

Table 1.   Dataset matrix for ITA strain and displacement measurements.

ITA State / Load Case	No Damage No hole (State 1)	3.175 mm / 1/8 inch hole (State 2)	6.350 mm / 2/8 inch hole (State 3)	9.525 mm / 3/8 inch hole (State 4)	12.700 mm / 4/8 inch hole (State 5)
Compression 2062g / 20.22N	S-1-C20 D-1-C20	S-2- C20 D-2-C20	S-3-C20 D-3-C20	S-4-C20 D-4-C20	S-5-C20 D-5-C20
Compression 1562g / 15.32N	S-1-C15 D-1-C15	S-2-C15 D-2-C15	S-3-C15 D-3-C15	S-4-C15 D-4-C15	S-5-C15 D-5-C15
Compression 1062g / 10.41N	S-1-C10 D-1-C10	S-2-C10 D-2-C10	S-3-C10 D-3-C10	S-4-C10 D-4-C10	S-5-C10 D-5-C10
Compression 0562g / 5.51N	S-1-C05 D-1-C05	S-2-C05 D-2-C05	S-3-C05 D-3-C05	S-4-C05 D-4-C05	S-5-C05 D-5-C05
No Load	S-1-NL0 D-1-NL0	S-2-NL0 D-2-NL0	S-3-NL0 D-3-NL0	S-4-NL0 D-4-NL0	S-5-NL0 D-5-NL0
Tension 0562g / 5.51N	S-1-T05 D-1-T05	S-2-T05 D-2-T05	S-3-T05 D-3-T05	S-4-T05 D-4-T05	S-5-T05 D-5-T05
Tension 1062g / 10.41N	S-1-T10 D-1-T10	S-2-T10 D-2-T10	S-3-T10 D-3-T10	S-4-T10 D-4-T10	S-5-T10 D-5-T10
Tension 1562g / 15.32N	S-1-T15 D-1-T15	S-2-T15 D-2-T15	S-3-T15 D-3-T15	S-4-T15 D-4-T15	S-5-T15 D-5-T15
Tension 2062g / 20.22N	S-1-T20 D-1-T20	S-2-T20 D-2-T20	S-3-T20 D-3-T20	S-4-T20 D-4-T20	S-5-T20 D-5-T20

strain data for damage state 1 (no damage) under a compression load of 20.22N, while "D-5-T15" refers to the displacement data for damage state 5 (12.7mm hole) under tensile load of 15.32N. The loads were produced by placing masses in a cradle suspended on the end of the wire connected to the bar as previously described. The masses ranged from 500 grams to 2000 grams, added in increments of 500 grams, with the cradle itself adding 62 grams. The number next to the load case in Table 1 corresponds to the mass used.

Each "S-…" data set in Table 1 contains thirty scans of fiber optic and foil strain data. Each "D-…" data set contains displacement measurements from the linear gauge and iFEM. Figure 8 plots the beam equation-derived
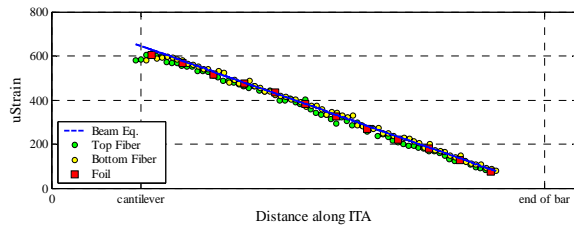

Figure 8. Strain data for No Damage (State1) with tension load of 20.22 N (2062 grams).
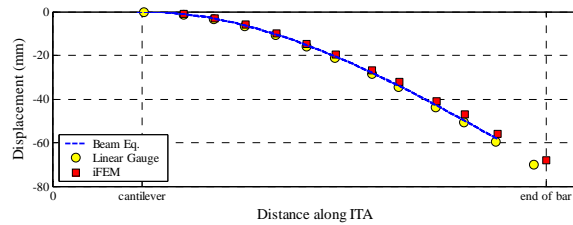

Figure 9. ITA displacement for No Damage subjected to tension load of 20.22 N (2062 grams).

4

strain versus the average measured strain from the top and bottom fiber segments and foil gauges for S-1-T20 (No damage – 2062g/20.22N tension load). Physical displacement measurements were obtained from the linear gauge at 13 locations. Figure 9 shows the average measured physical displacements versus the beam equation-derived displacements for the same load condition as Fig. 8. These plots show agreement between the measured data and the analytical results, which were based on standard cantilevered beam theory.

V. Structural Anomaly Detection Technique

Figures 10-14 show, for each damage state, the shape of the ITA as given by standard cantilevered beam theory, physical measurement, and iFEM prediction with the ITA subjected to a compression load of 20.22N. All three are
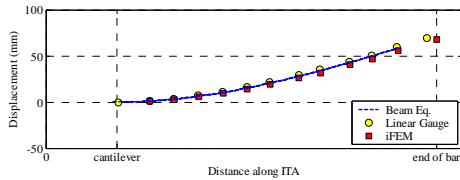
Figure 10.   Displacement for No Damage state with 20.22N compression-load. (D-1-C20)
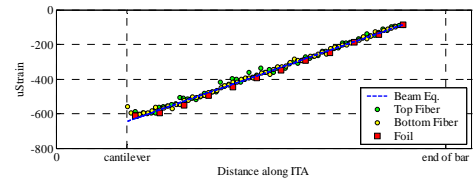
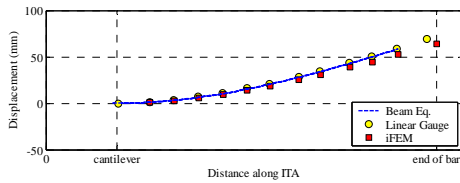**Figure 15.   Strain for State 1 (no damage) with 20.22N compression load (S-1-C20).**

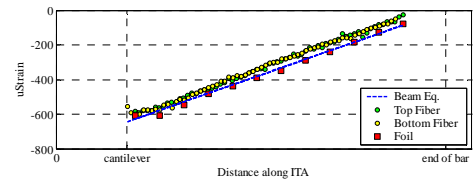**Figure 11.   Displacement for State 2 with 20.22N compression load (D-2-C20).**

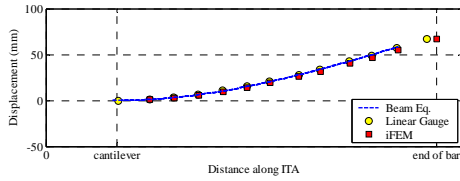**Figure 16.   Strain for State 2 with 20.22N compression load (S-2-C20).**

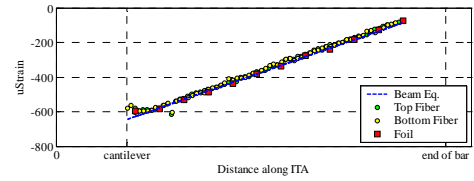**Figure 12.   Displacement for State 3 with 20.22N compression load (D-3-C20).**

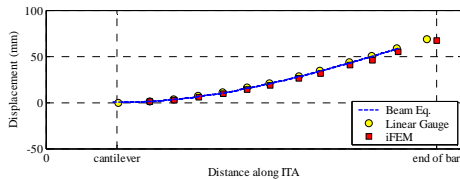**Figure 17.   Strain for State 3 with 20.22N compression load (S-3-C20).**

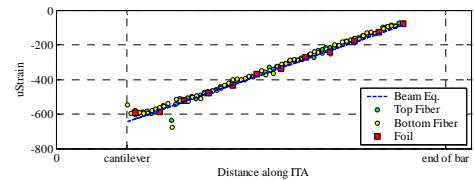**Figure 13.   Displacement for State 4 with 20.22N compression load (D-4-C20).**

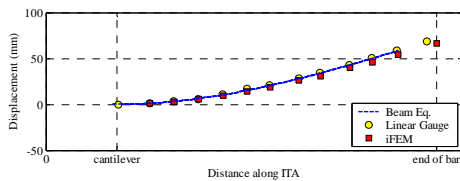**Figure 18.   Strain for State 4 with 20.22N compression load (S-4-C20).**

Figure 14.   Displacement for State 5 with 20.22N compression load (D-5-C20).
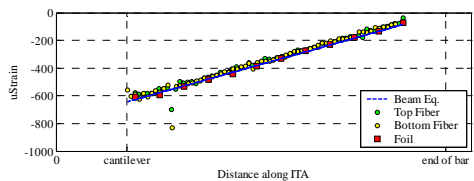

Figure 19.   Strain for State 5 with 20.22N compression load (S-5-C20).

in general agreement, and there is no observable localized deviation as the damage state progresses – the effect of the damage does not appear to impact the overall surface shape of the ITA.

Figure 15-19 show sequential plots of the beam equation-derived strain versus the average measured strain for the five damage states with the ITA subjected to same load as Fig. 10-14. The two gratings near the damage site show a trend of successively larger strain deviations (Fig. 16-19) from the non damage state (Fig. 15). A similar trend was observed for all other load cases. The close proximity of the strain deviation location to the damage site suggests that an analytical technique may be devised to detect and locate structural anomalies based on strain data.

By establishing limits on the magnitude of strain deviations based on the no damage state, an anomaly detection technique based on the frequency of excursions from the limits is proposed. Because the cantilevered ITA is expected to have a linear strain profile, strain deviation limits were established based on statistical deviation from a linear curve fit for each load case in the no damage state. Figure 20 shows, for the no-damage test data, the zero-mean plot and a proposed ±50.33 μstrain limit which is a ±3 sigma band based on the maximum sigma of 16.77

μstrain observed over the 270 scans. Due to bonding or fabrication irregularities, a few sensors exhibited variances exceeding the ±3 sigma band in the no damage case. These variances may impact the anomaly detection performance.

Anomalies are detected by counting the number of times that an individual strain sensor exceeds these limits (pop count) over some prescribed number of consecutive scans (scan history). In this analysis, the scan history size was set at 18, and the pop count was set at 7. This means that if, over 18 consecutive scans, a sensor exceeded these limits 7 or more times, a possible structural anomaly may be present in the vicinity of the sensor.
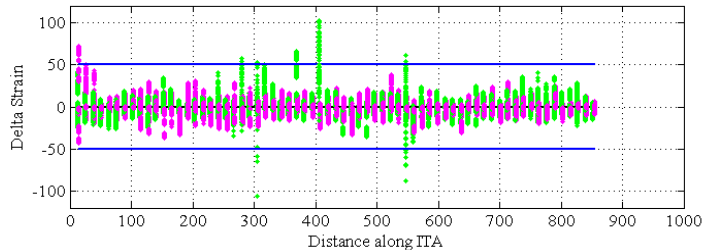

Figure 20. **Zero-mean plot of all load cases for the no damage state used to establish limit bands. Deviation from linear fit is shown in green for the top fiber and magenta for the bottom fiber. The blue line shows the ±3 sigma band limit.**

VI.   Test Results

The anomaly detector was applied to the damage data detailed in table 1. To simulate a flight environment, the data was presented to the detector in increasing order of damage (from S1 to S5) with the load cases for each damage state selected at random – all load cases for a damage state were processed before proceeding to the next level of damage.

The anomaly detector results are shown in Fig. 21-25. Figure 21 shows that the detector found no candidates in the non-damage state of the ITA. In Fig. 25, which shows the extreme damage case, the detector highlights two sensors that may be in the vicinity of structural damage. Moreover, the fact that one of the highlighted sensors is from the top fiber (located at x=139.25mm, y=41.27mm), and the other from the bottom fiber (located at x=140.95mm, y=22.23mm), suggests that there is a single candidate damage site located between the sensors (x=140.10mm, y=31.75mm). The locations of these sensors are highlighted on a diagram of the damaged ITA in Fig. 26, which shows a reasonable correspondence between the detector-calculated location of possible damage and the actual location of the drilled hole. As previously noted in Fig. 10-14, the iFEM results confirm that the detector results are not due to localized shape deformation.
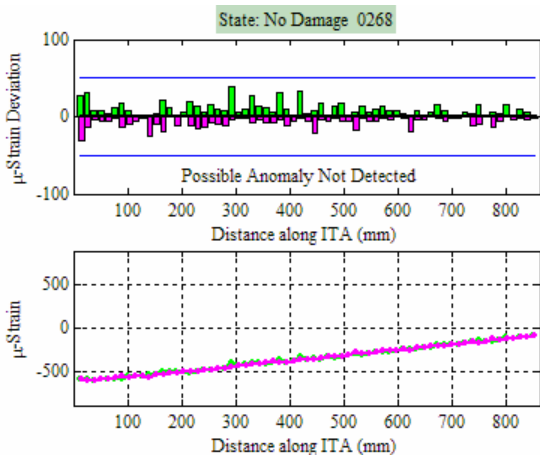
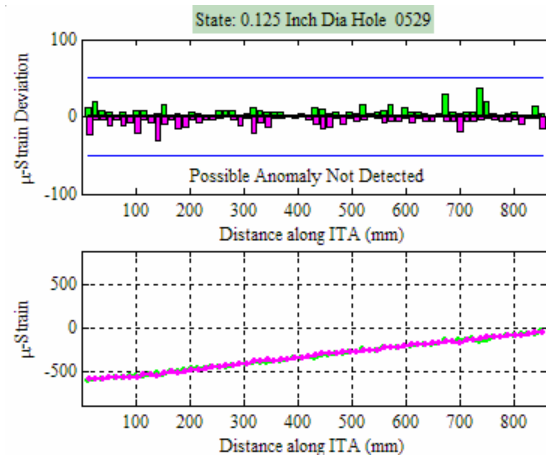**Figure 21.** Detector display for a damage state 1 case.

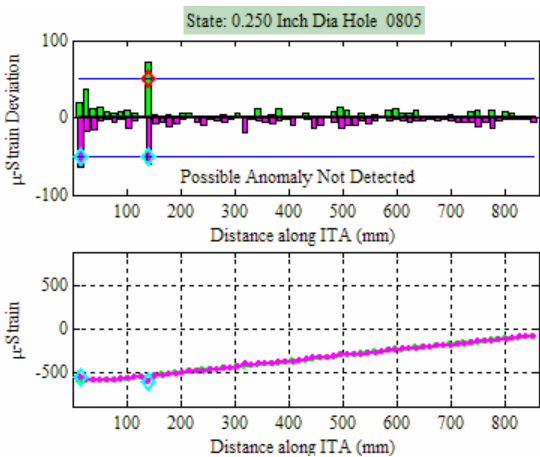**Figure 22.** Detector display for a damage state 2 case.

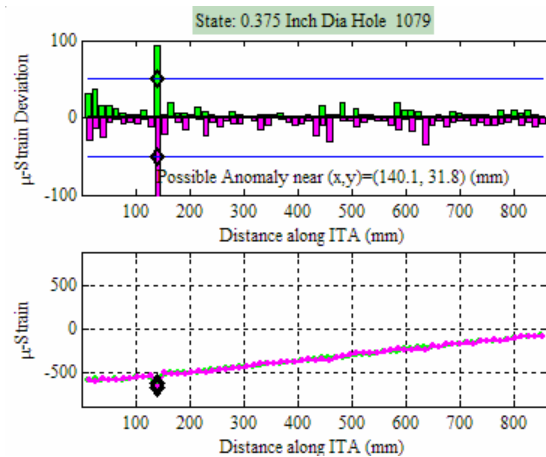**Figure 23.** Detector display for a damage state 3 case.

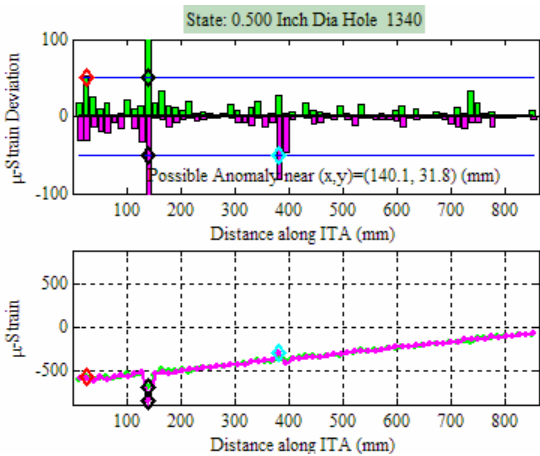**Figure 24.** Detector display for a damage state 4 case.

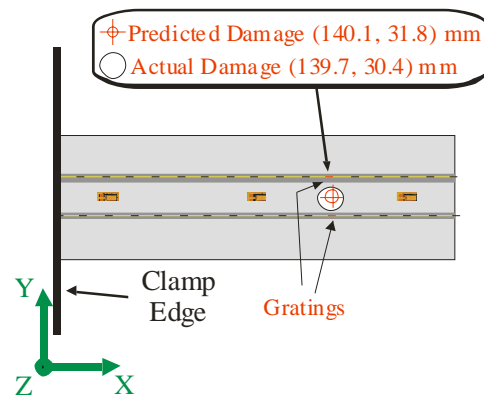**Figure 25.** Detector display for a damage state 5 case.

Figure 26. Short section of the bar showing locations of gratings that triggered the detector and the predicted damaged relative to the actual damage site.

American Institute of Aeronautics and Astronautics

VII.   Conclusion

This paper proposes a technique that uses densely distributed fiber optic strain sensors and an inverse finite element method as the basis for a novel detection algorithm that identifies potential structural anomalies. The technique was successfully applied to a series of laboratory tests conducted on a test coupon subjected to increasing levels of damage. Issues that need to be addressed include improving the sensor application techniques for increased strain accuracy and replacing the linear displacement probe with a non-contact sensor. Future research opportunities include investigating the effects of alternative sensor density and layout schemes, investigating the performance of the technique on different damage types (drill, puncture, fatigue crack growth, multi-site, etc.), characterizing the relationship between the three major parameters of the method (band limit, pop count, and scan history size) to the anomaly detection performance, and applying the technique to more complex structures and loading profiles.

References

[1]Froggatt, M. E., and Moore, J. P., "Distributed Measurement of Static Strain in an Optical Fiber with Multiple Bragg Gratings at Nominally Equal Wavelengths," *Applied Optics-OT*, Vol. 37, No. 10, 1998, pp. 1741.

[2]Quach, C. C., and Vazquez, S. L., "Comparison of Fiber Strain Demodulation Implementations," NASA TM-2005-0213521, 2005.

[3]Childers, B. A, Froggatt, M. E., Allison, S. G., and Moore, T. C., Sr., Hare, D. A., Batten, C. F. and Jegley, D. C., "Use of 3000 Bragg Grating Strain Sensors Distributed on Four Eight Meter Optical Fibers During Static Load Tests of a Composite Structure," NASA-2001-9spie-bac, 2001.

[4]Munns, T. E., Kent, R. M., et al., "Health Monitoring for Airframe Structural Characterization", NASA CR-2002-211428, 2002.

[5]Tessler, A., Spangler, J. L., "A Least-Squares Variational Method for Full-Field Reconstruction of Elastic Deformations in Shear Deformable Plates and Shells," Computer Methods in Applied Mechanics and Engineering, Vol. 194, pp. 327-339, 2005.

[6]Tessler, A. and Spangler, J. L., "Inverse FEM for Full-Field Reconstruction of Elastic Deformations in Shear Deformable Plates and Shells," Proceedings of Second European Workshop on Structural Health Monitoring, Munich, Germany, pp. 83-90, 2004.

[7]Vazquez, S. L., Tessler, A., Quach, C. C., Cooper, E. G., Parks, J., Spangler, J. L., "Structural Health Monitoring Using High-Density Fiber Optic Strain Sensor and Inverse Finite Element Methods", NASA TM-2005-213761, 2005.

[8]Tessler, A., Spangler, J., L., "A Variational Principal for Reconstruction of Elastic Deformation of Shear Deformable Plates and Shells", NASA TM-2003-212445.